Eur Radiol (2017) 27:4461–4471
DOI 10.1007/s00330-017-4811-2

HEPATOBILIARY-PANCREAS

Gadoxetic acid disodium-enhanced MR imaging of cholangiolocellular carcinoma of the liver: imaging characteristics and histopathological correlations

Hiroki Haradome[1] · Toshiyuki Unno[2] · Hiroyuki Morisaka[3] · Yusuke Toda[1] · Thomas C. Kwee[4] · Hiroshi Kondo[5] · Keiji Sano[6] · Tomoaki Ichikawa[3] · Fukuo Kondo[7] · Masahiko Sugitani[8] · Tadatoshi Takayama[9]

Received: 25 November 2016 / Revised: 3 March 2017 / Accepted: 13 March 2017 / Published online: 24 April 2017
© European Society of Radiology 2017

Abstract

Objectives To review the gadoxetic acid disodium (EOB)-enhanced magnetic resonance (MR) imaging features of cholangiolocellular carcinoma (CoCC) of the liver and compare them with those of hepatocellular carcinoma (HCC) and intrahepatic cholangiocarcinoma (ICC).

Methods EOB-enhanced MR images of 19 patients with CoCC, 23 with ICC, and 51 with HCC were retrospectively evaluated qualitatively and quantitatively. Univariate and multivariate analyses were performed to determine the characteristic MR features of CoCC with histopathological–imaging correlation.

Results Multivariate logistic regression analysis showed that dot-/band-shaped internal enhancement during the arterial and portal phases ($P < 0.001$), and larger arterial ring enhancement ratio (CoCC, 0.13 ± 0.04; ICC, 0.074 ± 0.04; $P = 0.013$) were significantly independently associated with CoCC in contrast to ICC, whereas several MR features including progressive enhancement during the portal and late phases ($P < 0.001$), target appearance in the hepatocyte phase ($P = 0.004$), and vessel penetration ($P = 0.013$) were significantly more frequently associated with CoCC than HCC. The dot-/band-like internal enhancement (78.9% of CoCCs) histopathologically corresponded to the tumour cell nest with vascular proliferations and retained Glisson's sheath structure.

Conclusions EOB-enhanced MR features of CoCC largely differ from those of HCC but are similar to those of ICC. However, the finding of thicker arterial ring enhancement with dot-/band-like internal enhancement could help differentiate CoCC from ICC.

Key Points

- *Gadoxetic acid-enhanced MR features of cholangiolocellular carcinoma (CoCC) resembled those of intrahepatic cholangiocarcinoma (ICC).*
- *Gadoxetic acid-enhanced MR features of CoCC largely differed from those of hepatocellular carcinoma.*
- *Dot-/band-like internal enhancement of CoCC may be helpful for differentiating from ICC.*
- *Arterial ring enhancement of CoCC was larger than that of ICC.*

Keywords Liver · Gadoxetic acid disodium-enhanced magnetic resonance imaging · Cholangiolocellular carcinoma · Intrahepatic cholangiocarcinoma Hepatocellular carcinoma

✉ Hiroki Haradome
karate.b@gmail.com

1 Department of Radiology, Nihon University School of Medicine, 30-1, Ohyaguchi Kami-cho, Itabashi-ku, Tokyo 173-8610, Japan

2 Department of Radiology, Showa General Hospital, Koganei, Japan

3 Department of Radiology, Saitama Medical University International Medical Center, Saitama, Japan

4 Department of Radiology, UMC Groningen, Groningen, The Netherlands

5 Department of Radiology, Teikyo University School of Medicine, Tokyo, Japan

6 Department of Surgery, Teikyo University School of Medicine, Tokyo, Japan

7 Department of Pathology, Teikyo University Hospital, Tokyo, Japan

8 Department of Pathology, Nihon University School of Medicine, Tokyo, Japan

9 Department of Digestive Surgery, Nihon University School of Medicine, Tokyo, Japan

Abbreviations

cHCC-CC	Combined hepatocellular and cholangiocarcinoma
CoCC	Cholangiolocellular carcinoma
DW	Diffusion-weighted
EOB	Gadoxetic acid disodium
HCC	Hepatocellular carcinoma
HE	Hematoxylin and eosin
ICC	Intrahepatic cholangiocarcinoma
LLC	Lesion-to-liver contrast
ROI	Region of interest
SI	Signal intensity
WHO	World Health Organization

Introduction

Cholangiolocellular carcinoma (CoCC), which was first reported by Steiner and Higginson in 1959 [1], is a rare malignant primary liver tumour. Formerly, CoCC was classified as a subtype of intrahepatic cholangiocarcinoma (ICC). However, based on distinct pathological characteristics, CoCC was recently categorized as a subtype of combined hepatocellular/cholangiocarcinoma with stem cell features (cholangiolocellular type) [2] according to the latest World Health Organization (WHO) classification criteria [3].

CoCC has been reported to have a better outcome after hepatectomy than other major primary malignant hepatic tumours such as hepatocellular carcinoma (HCC) and ICC [3, 4]. The reported 5-year survival rate in patients with CoCC who have undergone curative surgery is 75%, which is considerably higher than in patients with the mass-forming type of ICC (33%, $P = 0.0005$) [4]. Therefore, its accurate diagnosis is crucial for determining prognosis and therapeutic planning.

Gadoxetic acid disodium (EOB)-enhanced magnetic resonance (MR) imaging provides both vascular phase images and hepatocyte phase images based on hepatocellular transporter, which may improve the evaluation of several types of hepatic tumour [5–12]. Because of its advantages, EOB-enhanced MR imaging has been widely applied for detailed examination of many kinds of hepatic tumour [5–12]. However, unenhanced MR imaging features of CoCC have been investigated in only one original research study [13], and EOB-enhanced MR imaging features have been described in only one case report so far [14]. Thus, EOB-enhanced MR imaging features of CoCC still need to be clarified.

The purpose of this study, therefore, was to review EOB-enhanced MR imaging findings of CoCC with histopathological correlation and to determine its characteristic features compared with those of HCC and ICC.

Materials and methods

Patients

Our institutional review board approved this retrospective study. Written informed patient consent was waived.

During the period of January 2009 to June 2016, 172 patients with a pathological diagnosis of CoCC, ICC or HCC were retrospectively identified by searching the pathology database (CoCC and ICC from several institutions; HCC from our hospital). Of these 172 patients, 79 were excluded for the following reasons: (1) a pathological diagnosis solely on the basis of percutaneous biopsy (51 patients), (2) a history of previous adjuvant therapy such as transcatheter arterial chemoembolization, chemotherapy or radiofrequency ablation prior to surgical treatment (19 patients), and (3) nonavailability of EOB-enhanced MR imaging (9 patients). Finally, 93 patients (66 men and 27 woman; age, mean ± standard deviation, 68.0 ± 10.5 years; age range 33–84 years) with 93 lesions (19 CoCC, 23 ICC, and 51 HCC) were enrolled in this study. Of the ICCs 4 were well differentiated, 17 moderately differentiated and 2 poorly differentiated, and of the HCCs 6 were well differentiated, 42 moderately differentiated and 3 poorly differentiated.

MR imaging

MR examinations were performed using a 1.5-T scanner with an eight-channel-system and an eight-channel phased-array coil, or a 3.0-T scanner with a 32-channel-system and a 32-channel phased-array coil. Following a dual-echo gradient spoiled echo (GRE) T1-weighted acquisition before contrast agent administration, dynamic MR imaging with a fat-saturated 3D-GRE sequence was performed after administration of EOB (Primovist; Bayer HealthCare, Berlin, Germany). EOB (0.025 mmol/kg) was administered intravenously at a rate of 1 mL/s with a power injector through a 20-gauge catheter inserted into an antecubital vein, followed by a 20-mL saline flush at the same injection rate. The scan delay for the arterial phase was adjusted by monitoring the intensity of the thoracic aorta with a fluorotriggering technique [15]. Fat-saturated EOB-enhanced 3D-GRE T1-weighted images were obtained in the appropriately triggered arterial phase, and in the portal venous (60 s), the late phase (180 s), and hepatocyte phase (20 min). Between the late and hepatocyte phases, respiratory-triggered fat-saturated fast spin-echo T2-weighted and breath-hold or navigator-triggered diffusion-weighted (DW) echoplanar images were additionally acquired. The MR parameters of each sequence are presented in Table 1.

Qualitative analysis of MR features

All MR images were retrospectively reviewed in consensus by two abdominal radiologists with 20 and 9 years of experience

Table 1 MR imaging parameters

Sequence	TR/TE (ms)	Flip angle (degrees)	Section thickness/gap (mm)	Field of view (mm)	Matrix size	*b*-value (s/mm^2)
1.5-T MR unit						
Dual echo GRE T1-W imaging	150–170/2.2 (out), 4.5 (in)	12	6/0	330–380	350 × 160	
FSE T2-W imaging	2,500–8,000/64	90	6/0	330–380	256 × 192	
DW imaging	3,000–10,000/73	90	6/0	330–380	256 × 160	0, 1,000
3D GRE fat-saturated T1-W imaging	3.8/1.9	12	5/2.5	330–380	256–224	
3.0-T MR unit						
Dual echo GRE T1-W imaging	6.2/2.1 (in), 4.2 (out)	15	6/0	330–380	350 × 160	
FSE T2-W imaging	2,500–8,000/64	90	6/0	330–380	256 × 192	
DW imaging	3,000–10,000/70	90	6/0	330–380	256 × 160	0, 1,000
3D GRE fat-saturated T1-W imaging	3.3/1.4	12	3.8/1.8	330–380	256–320 × 192–224	

T1-W T1-weighted, *T2-W* T2-weighted, *DW* diffusion-weighted, *GRE* gradient echo, *FSE* fast spin echo

in hepatobiliary imaging, respectively, who were blinded to the clinical information and histological results, using a Picture Archiving and Communication System. Both the morphological features and EOB enhancement patterns during dynamic vascular and hepatocyte phases of all lesions were assessed. For morphological lesion assessment, the following items were evaluated: (a) the shape of the margins as well-defined, ill-defined (irregular) or lobulated, and signal intensity (SI) on T1-weighted, T2-weighted, and DW images relative to the hepatic parenchyma (hypointensity, isointensity or hyperintensity), (b) the presence of capsule formation or fat signal in the lesion, and (c) coexisting distal intrahepatic dilatation or liver capsular retraction.

For lesion enhancement assessment, the following items were evaluated: (d) appearance of arterial phase enhancement (ring or global), (e) enhancement pattern from arterial to late phases (washout or gradual), (f) presence of dot-/band-shaped internal enhancement in the arterial and/or late phases, (g) shape and SI relative to the hepatic parenchyma in the hepatocyte phase (low intensity, isointensity, partial or whole high intensity, or higher signal of the lesion center, i.e. EOB target sign), and (h) presence of penetrating vessels in the lesion. The EOB target sign was defined as a lesion showing isointensity or hyperintensity relative to the liver parenchyma at its center and hypointensity at its periphery on hepatocyte phase images [16]. In addition to evaluating the presence of arterial ring enhancement, dot-/band-like enhancement, which was defined as an area of nodular or thick line-shaped internal mass-enhancement during the arterial and late phases, was assessed to analyze complex enhancement characteristics of CoCC and ICC.

Quantitative analysis of EOB-enhanced MR imaging

For quantitative image analysis, the SI of all lesions and liver background and the thickness of arterial ring enhancement and the maximum diameter of CoCCs and ICCs were measured by another radiologist with 5 years of clinical experience, who was blinded to the pathological results. A circular region of interest (ROI) was placed over each entire lesion on serial EOB-enhanced MR images in the precontrast, dynamic, and hepatocyte phases. Liver parenchymal intensity near the lesion was measured using a fixed-sized circular ROI (100 mm^2) while avoiding major vessels and artifacts. On the basis of these measurements, the lesion-to-liver contrast (LLC) ratio was calculated using the following formula: $[(SI_{lesion}-SI_{liver})/SI_{muscle}]$, where SI_{lesion}, $SI_{liver,}$ and SI_{muscle} are the SIs of the lesion, liver and iliopsoas muscle on each image in the precontrast, dynamic and hepatocyte phases. The measured thickness of arterial ring enhancement of CoCCs and ICCs in each tumour was divided by their maximum diameter and expressed as the arterial ring enhancement ratio.

Pathological diagnosis

Pathological diagnosis of CoCC was established according to characteristic histopathological features on both hematoxylin and eosin (HE) staining and immunohistochemical staining according to the latest WHO criteria [3]. The characteristic HE histopathological features of CoCC include (a) small uniform glands that are arranged in a tubular, cord-like or "antler-like" anastomosing pattern with marked fibrous stroma, (b) continuous tumour cords with normal liver cell cords in a replacing growth pattern, and (c) no mucin production. The tumour cells are immunochemically positive for biliary/hepatocyte progenitor cell markers. Further histological analyses including imaging–pathological correlation were conducted by a pathologist with over 20 years of experience in hepatobiliary pathology.

Statistical analysis

The differences in mean age of the three patient groups were evaluated using a *t* test and the differences in lesion size between CoCC and ICC and between CoCC and HCC were evaluated using the Mann-Whitney test. The differences in gender distribution among the CoCC, ICC and HCC patient groups were evaluated using Pearson's chi-squared test. The variances in clinical background and the results of the qualitative MR features between CoCC and ICC patients and between CoCC and HCC patients were compared using Fisher's exact test with Bonferroni correction. The parameters found to have statistical significance in a univariate analysis were entered into a multiple logistic regression model to identify the imaging findings useful for differentiating CoCC from ICC and HCC. Both univariate and multiple logistic regressions were analyzed using the Firth method. Differences in ring enhancement ratio between CoCC and ICC lesions were evaluated using the Mann-Whitney *U* test. This significance test was not used for the HCC data because no HCC showed arterial ring enhancement. *P* values <0.05 were considered to indicate a significant difference.

Results

Patient characteristics and clinical background

Patient characteristics and clinical background are shown in Table 2. There were no significant differences in mean age between CoCC patients and ICC patients, or in gender distribution and mean lesion size among the three groups of patients (CoCC, ICC, HCC), although there was a significant difference in mean age between CoCC patients and HCC patients. With regard to chronic liver disorders, 10 CoCC patients (52.6%), 6 ICC patients (26.1%) and 47 HCC patients (92.2%) had liver disorders, and 9 CoCC patients (47.4%), 16 ICC patients (69.6%) and 4 HCC patients (7.4%) did not have liver disorders. With regard to HBV and HCV infection, 47.4% of CoCC patients and 82.6% of ICC patients were negative, and 78.4% of HCC patients were positive. With regard to tumour markers including AFP and PIVKA-II, 36.8% of CoCC patients and 39.1% of ICC patients were negative, and 82.4% of HCC patients were positive.

Table 2 Patient characteristics and clinical background

	CoCC (*n* = 19)	ICC (*n* = 23)	HCC (*n* = 51)	*P* value	
				CoCC vs. ICC	CoCC vs. HCC
Mean age (years)	62.2[a]	68.3	69.9	0.44	0.002
Age range (years)	41–84	45–81	33–84		
Sex ratio (M:F)	12:7	17:6	37:14	0.453	0.446
Mean lesion size (mm)	43.6	30.3	37.6	0.072	0.202
Background liver, *n* (%)					
Liver cirrhosis	2 (10.5)	3 (13.0)	11 (21.6)	1.000	0.981
Chronic hepatitis	8 (42.1)	3 (13.0)	36 (70.6)	0.085	0.100
Fatty liver	2 (10.5)	1 (4.3)	1 (2.0)	1.000	0.354
Normal liver	9 (47.4)[a]	16 (69.6)	4 (7.8)	0.418	0.001
Hepatic viruses, *n* (%)					
HBV	7 (36.8)	2 (8.7)	16 (31.4)	0.111	1.000
HCV	3 (15.8)	2 (8.7)	24 (47.1)	1.000	0.052
Negative	9 (47.4)[b]	19 (82.6)	13 (25.5)	0.046	0.308
Tumour markers, *n* (%)[c]					
AFP	4 (21.1)	1 (6.30)	10 (43.5)	0.316	0.514
PIVKA-II	3 (15.8)[a]	0 (0)	14 (60.9)	0.169	0.001
CA19-9	8 (42.1)	7 (43.8)	3 (13.0)	1.000	0.140
CEA	3 (15.8)	1 (6.30)	5 (21.7)	1.000	1.000
Negative	7 (36.8)	9 (39.1)	9 (17.6)	1.000	0.227

CoCC Cholangiolocellular carcinoma, *ICC* Intrahepatic cholangiocarcinoma, *HCC* Hepatocellular carcinoma, *HBV* Hepatitis B virus, *HCV* Hepatitis C virus, *AFP* Alpha-fetoprotein, *PIVKA-II* Protein induced by vitamin K antagonist-II, *CA-19-9* Cancer antigen-19-9, *CEA* Carcinoembryonic antigen

[a] There were significant differences in mean age, normal background liver and PIVKA-II positivity between CoCC and HCC

[b] There was significant differencein hepatic virus negativity between CoCC and ICC patients

[c] Several types of tumour markers were positive in five patients with CoCC, in three with ICC, and in 22 with HCC

Qualitative MR features

The morphological and EOB enhancement MR features of CoCC, ICC, and HCC are shown in Tables 3 and 4. Most CoCCs and ICCs appeared as lobulated masses (68.4% and 69.6%, respectively) (Figs. 1, 2, and 3), and there was a significant difference in the frequency of this finding between CoCCs and HCCs ($P < 0.001$). None of the CoCCs or ICCs had any capsule formation or intralesional fat signal, in contrast to the presence of these findings in HCCs ($P < 0.05$). Capsular retraction due to fibrous contraction was seen in 26.3% of CoCCs and in 17.4% of ICCs. Peripheral intrahepatic bile duct dilatation was seen in 47.8% of ICCs (Fig. 3), and there was a significant difference in the frequency of this finding between CoCCs and ICCs ($P = 0.035$). The majority of CoCCs and ICCs demonstrated arterial ring enhancement with delayed progression (Figs. 1, 2, and 3), and there was a significant difference in the frequency of this finding between CoCCs and HCCs ($P < 0.001$). Dot-/band-like internal enhancement was seen in 78.9% of CoCCs during the arterial and late phases (Figs. 1 and 2), and there were significant differences in the frequency of this finding between CoCCs and the other tumour types ($P < 0.001$). "HCC-like" global arterial enhancement was seen in 4 CoCCs (21.1%) and 5 ICCs (21.7%; Fig. 4). The EOB target sign was seen in 84.2% of CoCCs (Figs. 1 and 2), and there were significant differences in the frequency of this finding between CoCCs and the other tumour types ($P < 0.01$). Vessel penetration into the lesion was seen at similar frequencies in CoCCs (31.6%) and ICCs (34.8%) (Fig. 3), while none of the HCCs showed this finding.

Significant MR features of CoCCs in the multivariate logistic regression analysis are shown in Table 5. In the

Table 3 Morphological MR imaging features

	CoCC ($n = 19$)	ICC ($n = 23$)	HCC ($n = 51$)	*P* value	
				CoCC vs. ICC	CoCC vs. HCC
Tumour margin					
Smooth	0 (0)	1 (4.3)	32 (62.7)	1.000	<0.001
Lobulated	13 (68.4)[a]	16 (69.6)	10 (19.6)		
Irregular	6 (31.6)[a]	6 (26.1)	9 (17.6)		
Capsule	0 (0)	0 (0)	34 (66.7)[a]	N/A	<0.001
Fat	0 (0)	0 (0)	13 (25.5)[a]	N/A	0.014
T1-W imaging lesion signal					
Low intensity	18 (94.7)[a]	23 (100)	31 (60.8[b]	0.905	0.034
Isointensity	1 (5.3)	0 (0)	16 (31.4)		
High intensity	0 (0)	0 (0)	4 (7.8)		
T2-W imaging lesion signal					
Low intensity	0 (0)	2 (8.7)	0 (0)	0.815	<0.001
Isointensity	0 (0)	0 (0)	8 (15.7)		
High intensity	19 (100)[a]	21 (91.3)	43 (84.3)		
Ring-like	6 (31.6)	4 (17.4)	0 (0)		
Entire	13 (68.4)	17 (73.9)	43 (84.3)		
DW imaging lesion signal ($b = 1{,}000$ s/mm^2)					
Low intensity	0 (0)	0 (0)	0 (0)	$P = 1.000$	$P < 0.001$
Isointensity	0 (0)	0 (0)	5 (9.8)		
High intensity	19 (100)[a]	23 (100)	46 (90.2)		
Target	11 (57.9)	10 (43.5)	0		
Entire	8 (42.1)	13 (56.5)	46 (90.2)		
Capsular retraction	5 (26.3)[a]	4 (17.4)	1 (2.0)	1.000	0.009
Intrahepatic duct dilatation	2 (10.5)	11 (47.8)[b]	3 (5.9)	0.035	1.000

The data are presented as number (%) of patients

CoCC Cholangiolocellular carcinoma, *ICC* Intrahepatic cholangiocarcinoma, *HCC* Hepatocellular carcinoma, *T1-W* T1-weighted, *T2-W* T2-weighted, *DW* Diffusion-weighted, *N/A* Not available

[a] There were significant differences in tumour margin, capsule, intratumoral fat, lesion signal on T1-W, T2-W and DW imaging, and capsular retraction between the CoCC and HCC patients

[b] There were significant differences in intrahepatic duct dilatation between the CoCC and ICC patients

Table 4 Qualitative Gd-EOB-DTPA enhancement MR imaging features

	CoCC ($n = 19$)	ICC ($n = 23$)	HCC ($n = 51$)	*P* value	
				CoCC vs. ICC	CoCC vs. HCC
Dynamic enhancement pattern					
Arterial phase					
Ring	15 (78.9)[a]	18 (78.3)	0 (0)	1.000	<0.001
Global	4 (21.1)	5 (21.7)	51 (100)[a]		
Portal and late phases					
Washout	2 (10.5)	4 (17.4)	46 (90.2)[a]	1.000	<0.001
Progressive enhancement	12 (63.2)[a]	16 (69.6)	0 (0)		
None	3 (15.8)	3 (13.0)	0 (0)		
Isointense	2 (10.5)	0 (0)	5 (9.8)		
Dot-/band-like enhancement	15 (78.9)[b]	2 (8.7)	0 (0)	<0.001	<0.001
Hepatocyte phase					
EOB target sign	16 (84.2)[b]	14 (60.9)	1 (2.0)	0.002	<0.001
Entirely low	3 (15.8)	9 (39.1)	39 (76.5)		
Partially high	0 (0)	0 (0)	10 (19.6)		
Isointense	0 (0)	0 (0)	1 (2.0)		
Vessel penetration	6 (31.6)[a]	8 (34.8)	0 (0)	1.000	$P < 0.001$
Arterial ring enhancement ratio	0.126 ± 0.05[c]	0.074 ± 0.04		0.005	

The data are presented as number (%) of patients

CoCC Cholangiolocellular carcinoma, *ICC* Intrahepatic cholangiocarcinoma, *HCC* Hepatocellular carcinoma

[a] There were significant differences in arterial phase enhancement, portal and late phase enhancement, and vessel penetration between the CoCC and HCC patients

[b] There were significant differences in dot-/band-like enhancement during portal and late phases and EOB target sign in the hepatocyte phase between the CoCC patients and the ICC and HCC patients

[c] There was a significant difference in arterial ring enhancement ratio between the CoCC and ICC patients

multivariate logistic regression analysis, dot-/band-shaped internal enhancement during the arterial and portal phases ($P < 0.001$), and larger arterial ring enhancement ratio ($P = 0.013$) remained as significant factors in predicting CoCC in contrast to ICC. Meanwhile, in the multivariate logistic regression analysis, a lobulated tumour margin ($P = 0.025$), capsular retraction ($P = 0.012$), target appearance on DW imaging ($P = 0.013$), arterial ring enhancement ($P < 0.001$), progressive portal and late phase enhancement ($P < 0.001$), dot-/band-shaped internal enhancement during the arterial and portal phases ($P < 0.001$), target appearance in the hepatocyte phase ($P = 0.004$), and vessel penetration ($P = 0.013$) remained as significant factors in predicting CoCC in contrast to HCC.

Quantitative analysis EOB-enhanced MR imaging

Temporal changes in LLC ratios of CoCCs, ICCs, and HCCs in each MR imaging phase are shown in Fig. 5. The temporal change in LLC ratio of CoCCs was similar to that of ICCs.

The SI of HCCs was markedly higher than in the liver in the arterial phase, rapidly decreased in the portal venous phase, and gradually decreased in the late and hepatobiliary phases. The LLC ratio of HCCs (mean ± standard deviation, 0.54 ± 0.40) in the arterial phase was significantly higher ($P < 0.01$) than that of CoCCs (-0.076 ± 0.66) and ICCs (-0.027 ± 0.50). The mean –LLC ratios of CoCCs (-1.19 ± 0.79) and ICCs (-1.07 ± 0.62) in the hepatobiliary phase were significantly lower ($P < 0.01$) than that of HCCs (-0.80 ± 0.50). The LCCs of the three tumour types in the precontrast, portal and late phases were not significantly different. A washout pattern was seen in only two CoCCs (10.5%) and four ICCs (17.4%), but in the majority HCCs (90.2%). The arterial ring enhancement ratio of CoCCs (0.13 ± 0.04) was significantly larger ($P = 0.005$) than that of ICCs (0.074 ± 0.04).

Imaging–histopathological correlations

All CoCCs appeared as grossly whitish solid masses without a fibrous capsule and microscopically showed no fat component

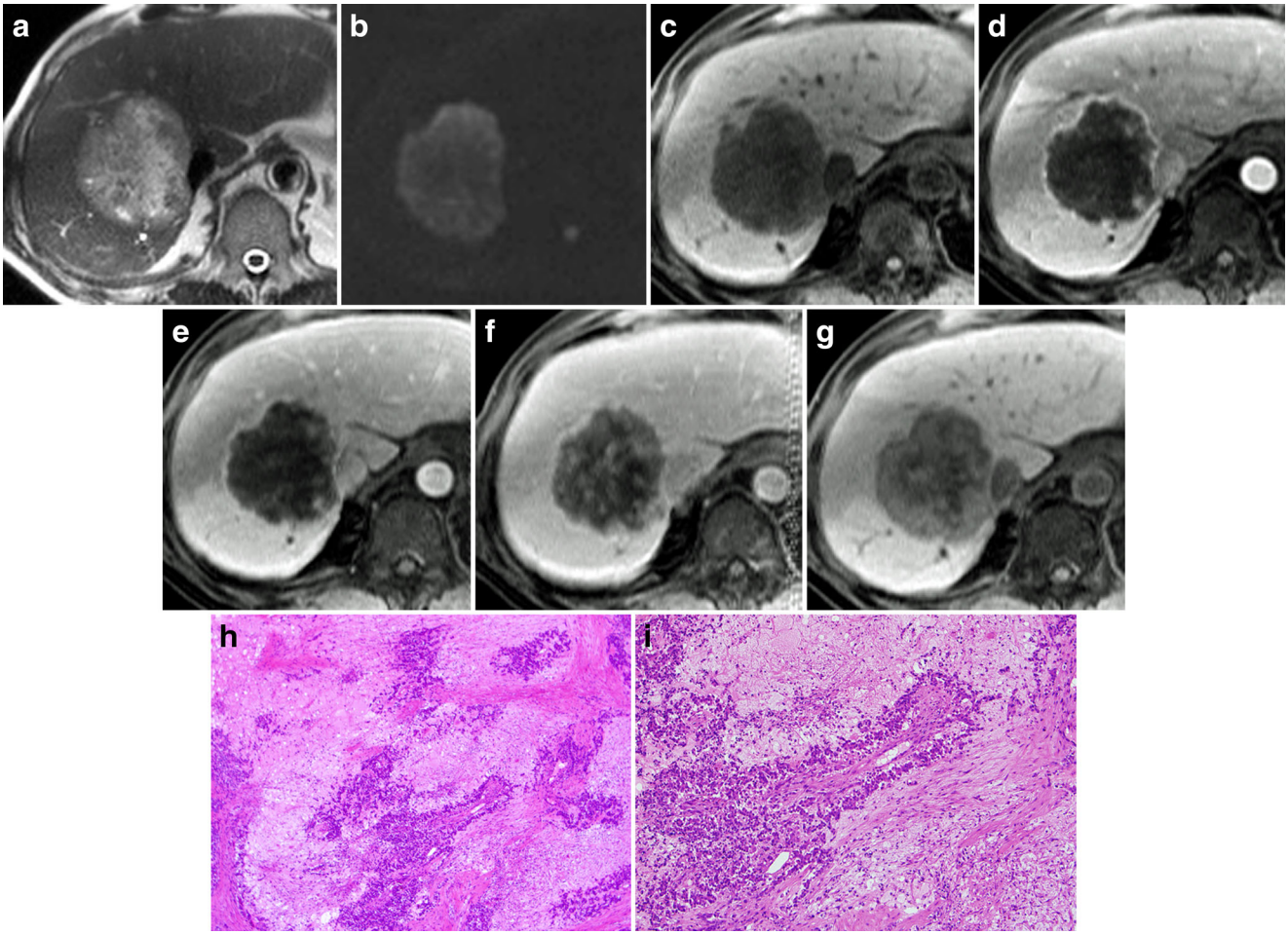

Fig. 1 A 69-year-old man with a CoCC before surgical resection. a Transverse T2-weighted image. b Transverse DW image with b-value of 1,000 s/mm2. c Transverse precontrast fat-saturated T1-weighted image. d–g Transverse Gd-EOB-DTPA-enhanced MR images (d arterial phase, e portal phase, f late phase, g hepatocyte phase). h, i Hematoxylin and eosin-stained sections at low power (h original magnification × 4) and high power (i original magnification × 10). A large lobulated mass located in the right hepatic lobe appears heterogeneously hyperintense on the T2-weighted (a) and DW (b) images, and heterogeneously hypointense on the precontrast fat-saturated T1-weighted image (c). The mass shows arterial ring enhancement with multiple dot-like internal enhancements (arrows) during the arterial and late phases (d–f). On the hepatocyte phase MR image (g) the mass has a target appearance (Gd-EOB-DTPA target sign), which corresponds to fibrous stroma on histopathology. The dot-like internal enhancement during the arterial and late phases on Gd-EOB-DTPA-enhanced MR images corresponds microscopically to the tumour cell nest with vascular proliferations (h, i)

or calcification. Peripheral highly cellular areas and central abundant hyalinized/edematous fibrotic stroma were seen in 15 CoCCs (78.9%), and this was reflected by arterial ring enhancement and the EOB target sign in the hepatocyte phase. Four CoCC lesions (21.1%) with global arterial enhancement consisted almost entirely of cellular components with only scant fibrotic stroma. Dot-/band-like internal enhancement during the arterial and late phases, which was observed in 15 CoCCs (78.9%), corresponded to the tumour cell nest with vascular proliferations and retained Glisson's sheath structure, respectively (Figs. 1 and 2). Four CoCCs showed areas of coagulation necrosis, and in two of these CoCCs, the necrotic change was widespread appearing as nonenhanced areas during dynamic phases of EOB-enhanced MR imaging. On the other hand, two ICC lesions showing dot-/band-like internal enhancement during the arterial and late phases had central necrosis or hyalinization with aggregated inflammatory cells (neutrophils, etc.).

Discussion

In this study, 78.9% of CoCCs showed arterial ring enhancement and 63.2% showed progressive delayed enhancement during the arterial and late phases on EOB-enhanced MR imaging (Figs. 1 and 2). This dynamic enhancement pattern on EOB-enhanced MR imaging is similar to that described in previous reports on contrast-enhanced CT/MR imaging with nonspecific extracellular contrast agents [13, 17, 18]. Similar arterial ring enhancement has been found CoCCs in

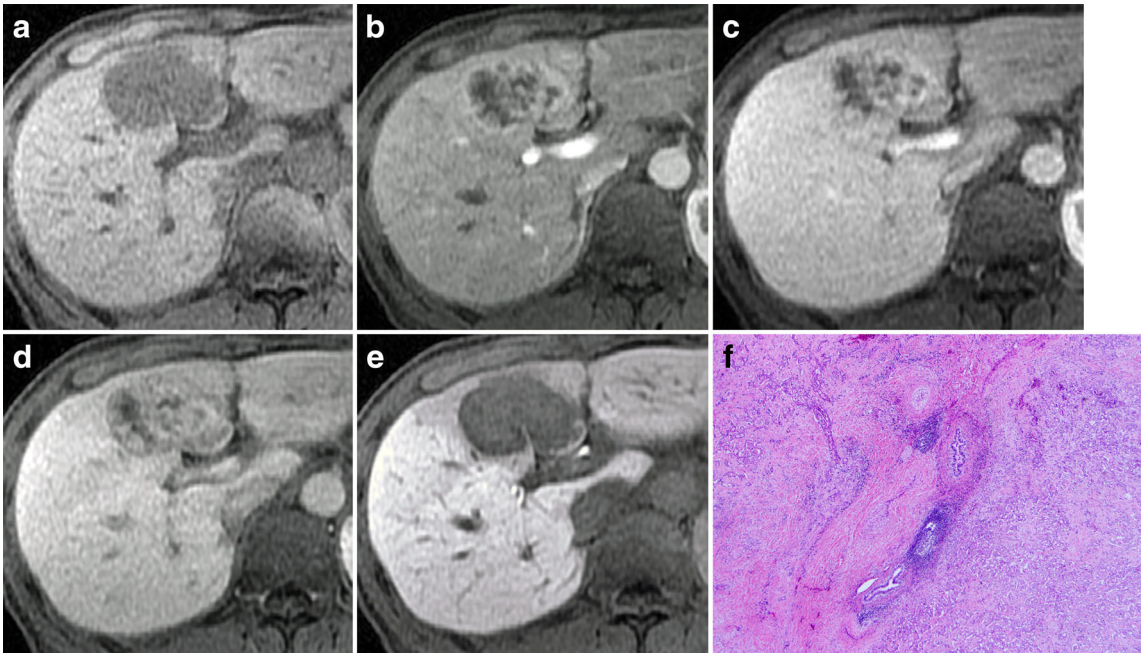

Fig. 2 A 50-year-old woman with a CoCC before surgical resection. a Transverse precontrast fat-saturated T1-weighted image. b–e Transverse Gd-EOB-DTPA-enhanced MR images (b arterial phase, c portal phase, d late phase, e hepatocyte phase). f Hematoxylin and eosin-stained section at low power (original magnification × 4). The lobulated mass located in the medial hepatic segment appears hypointense on the precontrast fat-saturated T1-weighted image (a) and shows relatively thick arterial ring enhancement with delayed progression during the arterial and late phases (b–d). Several dot-/band-like internal enhancements are also seen in the mass during the same phases (b–d). On the hepatocyte phase MR image the mass has a target appearance (Gd-EOB-DTPA target sign) due to central fibrous stroma. The hematoxylin and eosin-stained section (f) shows a retained Glisson's sheath structure in the fibrous stroma, which corresponds to the band-like internal enhancement during the arterial and late phases

previous studies (two of two, 100% [17], three of five, 60% [18], and six of eight, 75% [13]), and around half of the CoCCs showed progressive delayed enhancement. Histopathologically, all CoCCs showing arterial ring enhancement, which was probably due to peripheral highly cellular areas and central abundant hyalinized/edematous fibrotic stroma as shown on histopathological examination. On the other hand, all HCCs showed

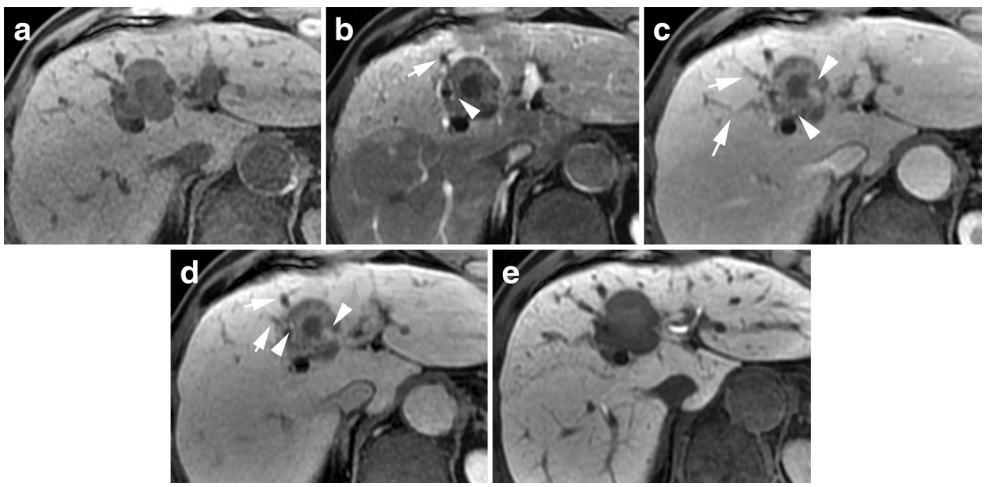

Fig. 3 A 64-year-old man with a moderately differentiated ICC before surgical resection. a Transverse precontrast fat-saturated T1-weighted image. b–f Transverse Gd-EOB-DTPA-enhanced MR images (b arterial phase, c portal phase, d late phase, e hepatocyte phase). The lobulated mass located in the medial hepatic segment appears hypointense on the pre-contrast fat-saturated T1-weighted image (a) and shows arterial ring enhancement with target-like internal enhancement, which has slightly progressed during the portal and late phases (b–d). Peripheral intrahepatic dilatation (arrows) and vessel penetration into the mass (arrowheads) are also seen during the arterial and late phases (b–d). The hepatocyte phase MR image (e) shows the mass to have a target appearance (Gd-EOB-DTPA target sign)

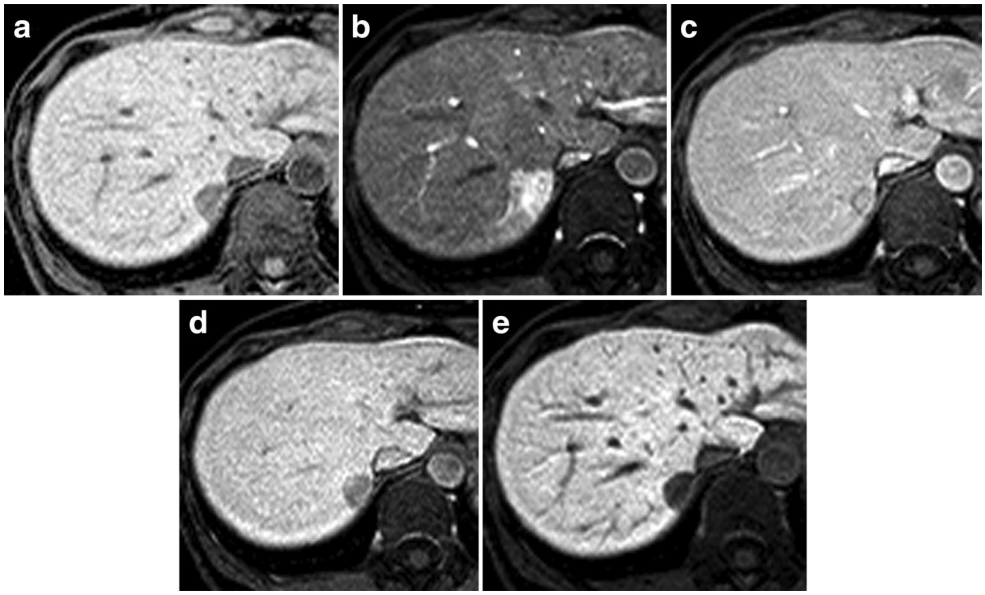

Fig. 4 A 55-year-old woman with a CoCC before surgical resection. a Transverse precontrast fat-saturated T1-weighted image. b–f Transverse Gd-EOB-DTPA-enhanced MR images (b arterial phase, c portal phase, d late phase, e hepatocyte phase). g Hematoxylin and eosin-stained section at high power. The slightly lobulated mass located in hepatic segment 7 (S7) appears heterogeneous and hypointense on the precontrast fat-saturated T1-weighted image (a), shows complete arterial enhancement and then becomes gradually hypointense compared to the hepatic parenchyma (pseudo washout) during the portal and late phases (b–d). This mass demonstrates no obvious target appearance on the hepatocyte phase MR image (e). On the hematoxylin and eosin-stained section, this mass consists mainly of cellular components and only scant central fibrotic stroma

global arterial enhancement and 87% exhibited late washout, as is widely known.

In this study, four CoCCs (21.1%), which predominantly consisted of highly cellular components and less fibrotic stroma on histopathological examination, showed global arterial enhancement, and of these, two were also hypointense during the portal and late phases (pseudo washout), thus resembling HCCs (Fig. 4). Although CoCCs show both ICC-like and HCC-like areas within the tumour and potentially demonstrate early arterial enhancement with late washout, this appears to occur in a minority of tumours. However, it may be hard to differentiate atypical CoCCs from HCCs without capsule and/or fat components preoperatively.

In addition, the majority (78.9%) of CoCCs showed dot-/band-like internal enhancement during the arterial and late phases (Figs. 1 and 2), and there were significant differences in the frequency of this finding between CoCCs and the other tumour types ($P < 0.001$), and this appearance was a significant factor in predicting CoCC in contrast to ICC and HCC in the multivariate logistic regression analysis. In terms of imaging–histopathological correlation, dot-like and band-like internal enhancement corresponded to the tumour cell nest with

Table 5 Significant MR features for CoCC in the multivariate logistic regression analysis

	Odds ratio (95% confidence interval)	*P* value
CoCC vs. ICC		
Dot-/band-like enhancement	146.5 ($10.6–3.62 \times 10^5$)	<0.001
Arterial ring enhancement ratio	5.10×10^{13} ($335.0–1.01 \times 10^{39}$)	0.013
CoCC vs. HCC		
Tumour margin (lobulated)	15.7 ($1.36–2.16 \times 10^3$)	0.025
Capsular retraction	30.4 (2.22–647.6)	0.012
DW imaging (target)	66.7 ($2.31–1.22 \times 10^3$)	0.013
Ring arterial enhancement	500 ($41.7–6.67 \times 10^4$)	<0.001
Progressive portal and late phase enhancement	1.30×10^3 ($57.6–9.29 \times 10^5$)	<0.001
Dot-/band-like enhancement	121 ($12.2–1.65 \times 10^4$)	<0.001
Hepatocyte enhancement (target)	47.6 (7.75–500)	0.004
Vessel penetration	250.2 ($2.31–1.22 \times 10^3$)	0.013

CoCC Cholangiolocellular carcinoma, *ICC* Intrahepatic cholangiocarcinoma, *HCC* Hepatocellular carcinoma

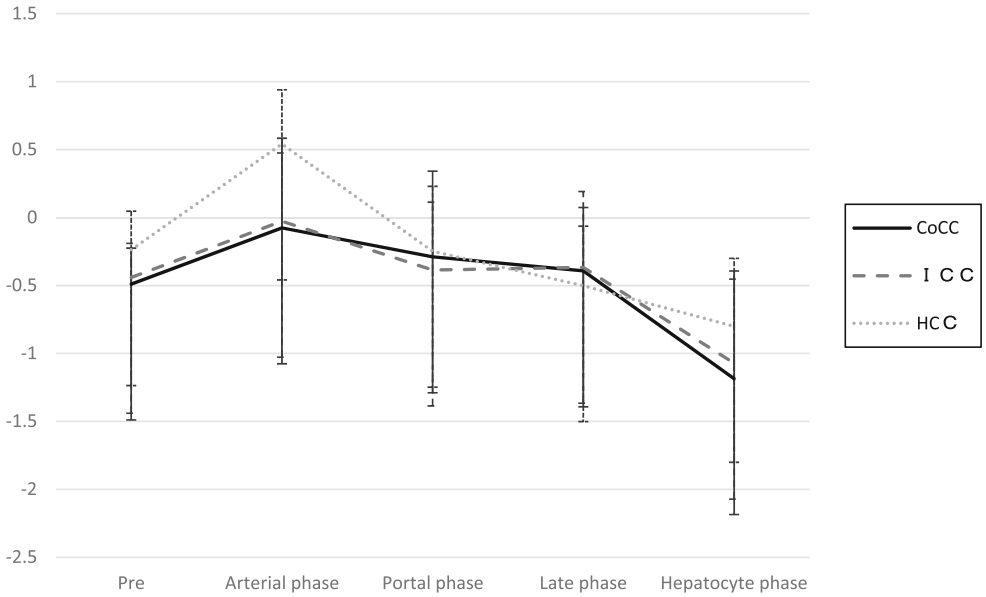

Fig. 5 LLC ratios for CoCCs, ICCs, and HCCs in each MR imaging phase. The temporal change in LLC ratio for CoCCs was similar to that for ICCs, but the signal intensity of ICCs in the arterial phase was slightly higher than that of the liver. The SI of HCCs in the arterial phase was markedly higher than that of the liver, rapidly decreased in the portal venous phase, and further gradually decreased in the late and hepatobiliary phases (*LLC* lesion-to-liver contrast, *CoCC* cholangiolocellular carcinoma, *ICC* intrahepatic cholangiocarcinoma, *HCC* hepatocellular carcinoma)

vascular proliferations and retained Glisson's sheath structure, respectively (Figs. 1 and 2).

Although ICCs have similar central fibrous stroma, there are some differences in the stroma between CoCCs and ICCs. The stromal fibrosis in ICCs tends to be more dense, which contributes to tumour aggressiveness and a poorer prognosis [19], while the stromal fibrosis in CoCCs is hyalinized/edematous and the tumour cell nests with vascular proliferations and varying degrees of necrotic changes are scattered within it [2], which explains the dot-like enhancement during the arterial and late phases. In addition, tumour cell nests in CoCCs are specifically arranged in the peripheral part of the tumour on histopathology, which seems to contribute to the larger arterial ring enhancement ratio than in ICCs. The finding of thin arterial ring enhancement is one of the characteristic features of ICCs [20]. Interestingly, we found that retained Glisson's sheath structure in the fibrous stroma of CoCCs corresponded to band-like enhancement during the arterial and late phases. Previous studies have demonstrated that portal/hepatic venous penetration into the tumour is a characteristic finding in CoCCs [13, 17, 18], and retention of normal hepatic tissue including Glisson's sheath also seems to be a characteristic feature of CoCCs.

We also found that CoCCs more frequently (84.2%) showed an EOB target sign than ICCs (60.9%) (Figs. 1 and 2). As previously reported in ICCs [19–22], histopathological analysis showed that the EOB target sign in CoCCs seems to be mainly formed by extracellular accumulation of EOB in stromal fibrosis. However, the EOB target sign has also been reported in other tumours including metastasis and scirrhous HCC [16, 23, 24]; thus this feature seems not to be specific for CoCCs.

EOB-enhanced MR features of CoCCs were considerably different from those in HCCs. Several MR features including progressive portal and late phase enhancement ($P < 0.001$), target appearance in the hepatocyte phase ($P = 0.004$), and vessel penetration ($P = 0.013$) were shown in the multivariate logistic regression analysis to occur significantly more frequently in CoCCs than in HCCs.

This study had several limitations. First, the study was retrospective and further prospective research is needed to confirm the results. Second, although CoCC is categorized as combined hepatocellular and cholangiocarcinoma (cHCC-CC) with stem cell features (cholangiolocellular type), discrimination of CoCC from the classical type of cHCC-CC requires further investigation because the prognosis of the classical type tends to be worse due to a higher risk of lymph node metastasis. Third, ROIs were not drawn separately on the central and peripheral portions of CoCCs and ICCs in this study. This measurement method may be more beneficial because central and peripheral areas generally contain different tissue components. However, such measurements were technically challenging and are prone to errors. Moreover, a previous study also adopted placement of the ROI at the largest diameter of the lesion for evaluating the enhancement characteristics of ICCs [21].

In conclusion, EOB-enhanced MR features of CoCCs largely differ from those of HCCs, but resemble those of ICCs. However, the finding of peripheral thicker arterial ring enhancement with dot-/band-like internal enhancement during the arterial and late phases could help differentiate CoCC from ICC.

Acknowledgements We are grateful to Kazuhito Nakayasu (Kondo Photo Process Co., Ltd.) for providing professional statistical advice.

Compliance with ethical standards

Guarantor The scientific guarantor of this publication is Tadatoshi Takayama

Conflict of interest The authors of this manuscript declare no relationships with any companies, whose products or services may be related to the subject matter of the article.

Funding The authors state that this work has not received any funding.

Statistics and biometry Kazuhito Nakayasu (Kondo Photo Process Co., Ltd.) kindly provided statistical advice.

Ethical approval Institutional Review Board approval was obtained.

Informed consent Written informed consent was waived by the Institutional Review Board.

Methodology
• Retrospective
• Case-control/observational study
• Multicenter study

References

1. Steiner PE, Higginson J (1959) Cholangiolocellular carcinoma of the liver. Cancer 12(4):753–759
2. Komuta M, Spee B, Vander Borght S et al (2008) Clinicopathological study on cholangiolocellular carcinoma suggesting hepatic progenitor cell origin. Hepatology 47(5):1544–1556
3. World Health Organization (2010) Classification of tumours of the digestive system, 4th edn. International Agency for Research on Cancer, Lyon
4. Ariizumi S, Kotera Y, Katagiri S et al (2014) Long-term survival of patients with cholangiolocellular carcinoma after curative hepatectomy. Ann Surg Oncol 21(Suppl 3):S451–S458
5. Ahn SS, Kim MJ, Lim JS, Hong HS, Chung YE, Choi JY (2010) Added value of gadoxetic acid-enhanced hepatobiliary phase MR imaging in the diagnosis of hepatocellular carcinoma. Radiology 255(2):459–466
6. Haradome H, Grazioli L, Tinti R et al (2011) Additional value of gadoxetic acid-DTPA-enhanced hepatobiliary phase MR imaging in the diagnosis of early-stage hepatocellular carcinoma: comparison with dynamic triple-phase multidetector CT imaging. J Magn Reson Imaging 34(1):69–78
7. Zech CJ, Grazioli L, Breuer J, Reiser MF, Schoenberg SO (2008) Diagnostic performance and description of morphological features of focal nodular hyperplasia in Gd-EOB-DTPA-enhanced liver magnetic resonance imaging: results of a multicenter trial. Invest Radiol 43(7):504–511
8. Grazioli L, Bondioni MP, Haradome H et al (2012) Hepatocellular adenoma and focal nodular hyperplasia: value of gadoxetic acid-enhanced MR imaging in differential diagnosis. Radiology 262(2):520–529
9. McInnes MD, Hibbert RM, Inácio JR, Schieda N (2015) Focal nodular hyperplasia and hepatocellular adenoma: accuracy of gadoxetic acid-enhanced MR imaging – a systematic review. Radiology 277(2):413–423
10. Palmucci S (2014) Focal liver lesions detection and characterization: the advantages of gadoxetic acid-enhanced liver MRI. World J Hepatol 6(7):477–485
11. Merkle EM, Zech CJ, Bartolozzi C et al (2016) Consensus report from the 7th international forum for liver magnetic resonance imaging. Eur Radiol 26(3):674–682
12. Neri E, Bali MA, Ba-Ssalamah A et al (2016) ESGAR consensus statement on liver MR imaging and clinical use of liver-specific contrast agents. Eur Radiol 26(4):921–931
13. Motosugi U, Ichikawa T, Nakajima H et al (2009) Cholangiolocellular carcinoma of the liver: imaging findings. J Comput Assist Tomogr 33(5):682–688
14. Kadono M, Kimura K, Imamura J et al (2011) A case of a large cholangiolocellular carcinoma. Clin J Gastroenterol 4(5):340–346
15. Haradome H, Grazioli L, Tsunoo M et al (2010) Can MR fluoroscopic triggering technique and slow rate injection provide appropriate arterial phase images with reducing artifacts on gadoxetic acid-DTPA (Gd-EOB-DTPA)-enhanced hepatic MR imaging? J Magn Reson Imaging 32(2):334–340
16. Granata V, Catalano O, Fusco R et al (2015) The target sign in colorectal liver metastases: an atypical Gd-EOB-DTPA "uptake" on the hepatobiliary phase of MR imaging. Abdom Imaging 40(7):2364–2371
17. Fukukura Y, Hamanoue M, Fujiyoshi F et al (2000) Cholangiolocellular carcinoma of the liver: CT and MR findings. J Comput Assist Tomogr 24(5):809–812
18. Asayama Y, Tajima T, Okamoto D et al (2010) Imaging of cholangiolocellular carcinoma of the liver. Eur J Radiol 75(1):e120–e125
19. Koh J, Chung YE, Nahm JH et al (2016) Intrahepatic mass-forming cholangiocarcinoma: prognostic value of preoperative gadoxetic acid-enhanced MRI. Eur Radiol 26(2):407–416
20. Kang Y, Lee JM, Kim SH, Han JK, Choi BI (2012) Intrahepatic mass-forming cholangiocarcinoma: enhancement patterns on gadoxetic acid-enhanced MR images. Radiology 264(3):751–760
21. Jeong HT, Kim MJ, Chung YE, Choi JY, Park YN, Kim KW (2013) Gadoxetate disodium-enhanced MRI of mass-forming intrahepatic cholangiocarcinomas: imaging-histologic correlation. AJR Am J Roentgenol 201(4):W603–W611
22. Kim SH, Lee CH, Kim BH et al (2012) Typical and atypical imaging findings of intrahepatic cholangiocarcinoma using gadolinium ethoxybenzyl diethylenetriamine pentaacetic acid-enhanced magnetic resonance imaging. J Comput Assist Tomogr 36(6):704–709
23. Ha S, Lee CH, Kim BH et al (2012) Paradoxical uptake of Gd-EOB-DTPA on the hepatobiliary phase in the evaluation of hepatic metastasis from breast cancer: is the "target sign" a common finding? Magn Reson Imaging 30(8):1083–1090
24. Park MJ, Kim YK, Park HJ, Hwang J, Lee WJ (2013) Scirrhous hepatocellular carcinoma on gadoxetic acid-enhanced magnetic resonance imaging and diffusion-weighted imaging: emphasis on the differentiation of intrahepatic cholangiocarcinoma. J Comput Assist Tomogr 37(6):872–881